



Article

Tribological Evaluation of Turbostratic 2D Graphite as Oil Additive

Halley Welther Jacques Dias^{1,2}, Alessandra Batista Medeiros¹, Cristiano Binder¹, João Batista Rodrigue Neto¹ , Aloísio Nelmo Klein¹ and José Daniel Biasoli de Mello^{1,2,3,*}

¹ Laboratório de Materiais, Departamento de Engenharia Mecânica, Universidade Federal de Santa Catarina, Florianópolis 88040-900, Brazil; halleydias@ifsc.edu.br (H.W.J.D.); alessandrabmedeiros@gmail.com (A.B.M.); cristiano.binder@labmat.ufsc.br (C.B.); joao.neto@labmat.ufsc.br (J.B.R.N.); a.n.klein@labmat.ufsc.br (A.N.K.)

² Instituto Federal de Ciência e Tecnologia de Santa Catarina, Campus Araranguá, Araranguá 88905-112, Brazil

³ Laboratório de Tribologia e Materiais, Universidade Federal de Uberlândia, Uberlândia 38400-902, Brazil

* Correspondence: ltm-demello@ufu.br or d.mello@labmat.ufsc.br; Tel.: +55-34-9-99293411

Abstract: In this study, powder technology was used to obtain Fe-SiC composites in which SiC particles act as precursors to generate a large amount of turbostratic graphite dispersed in the composite matrix. The selection of the alloy composition was studied employing Thermo-Calc[®] software to obtain the temperature and composition range for the stabilization of the graphite phase in iron with a high yield. The extracted turbostratic 2D graphite particles were dispersed in mineral oil in order to evaluate the potential of these particles as a lubricating oil additive. The structure and morphology of the extracted graphite were examined by Raman spectroscopy and transmission electron microscopy (TEM), indicating the highly disordered nature of turbostratic graphite. Reductions in the friction coefficient and wear rate of a tribological pair were observed when compared to the pure mineral oil and mineral oil with commercial graphite particles added. The misorientation and increase in interplanar distances of turbostratic 2D graphite induce a low degree of interaction between these atomic planes, which contributes to the low-friction coefficient and the lower wear rate obtained for this system.

Keywords: turbostratic graphite; lubricant additive; solid lubricant; friction; wear; nanoparticle



Citation: Dias, H.W.J.; Medeiros, A.B.; Binder, C.; Rodrigue Neto, J.B.; Klein, A.N.; de Mello, J.D.B. Tribological Evaluation of Turbostratic 2D Graphite as Oil Additive. *Lubricants* **2021**, *9*, 43. <https://doi.org/10.3390/lubricants9040043>

Received: 16 March 2021

Accepted: 13 April 2021

Published: 15 April 2021

Publisher's Note: MDPI stays neutral with regard to jurisdictional claims in published maps and institutional affiliations.



Copyright: © 2021 by the authors. Licensee MDPI, Basel, Switzerland. This article is an open access article distributed under the terms and conditions of the Creative Commons Attribution (CC BY) license (<https://creativecommons.org/licenses/by/4.0/>).

1. Introduction

The severity of tribological contact imposes limits in controlling the energy-efficiency performance of modern systems [1]. In particular, severe operating conditions with higher speeds and smaller clearances of interfaces that are in contact require high strength of the tribological pair to achieve higher energy efficiency [2]. In this context, intense investigation and research has been directed toward the development of new contact materials [1,2]. The combination of solid and liquid lubrication may be one of the most promising choices for controlling friction and wear in sliding tribological pairs. Indeed, effective control of friction and wear contributes to increasing the energy efficiency of modern mechanical systems [1–5].

Several inorganic materials are lamellar solid lubricants (MoS₂, WS₂, HBN, H₃O₃, GaSe, GaS, SnSe), and the most important are carbon-based materials [6–8]. Graphite is a lamellar solid composed entirely of carbon, which under appropriate conditions provides low friction and high wear resistance to sliding surfaces. Furthermore, it is an abundant mineral in nature, with low cost, and is used in many industrial applications [9]. Interest in the study of carbon-based materials is motivated by their capacity to hybridize in sp, sp² and sp³ [10]. Graphite, diamond, graphene, fullerene and carbon nanotubes, among other materials, are composed entirely of carbon, presenting different physical and chemical properties [11]. Graphite is organized in layers or lamellae with a hexagonal arrangement of covalent bonds, exhibiting van der Waals bonds between the lamellae or

layers [12]. This lamellar characteristic is one of the factors that make graphite a material with lubricant properties. Graphite can be formed with a well-organized structure in which the distance between lamellae does not show a significant variation. It can also exhibit an amorphous structure and present a disordered intermediate structure, known as turbostratic graphite [13]. In turbostratic graphite (TG), the lamellar stacking disorder confers lower shear strength between the lamellae compared to crystalline or tridimensional graphite, providing a low friction coefficient [12].

Recently, researchers [1–3,5,14] have identified and characterized turbostratic 2D graphite in self-lubricating materials in the form of in situ generated second-phase particles in the volume of a material developed. Binder [15] achieved success in developing a ferrous alloy of high strength with graphite nodules derived from the precursor SiC. These nodules are formed in situ in the metallic matrix volume and were characterized as having a turbostratic structure by Consoni [16] and Binder et al. [17]. Such studies have opened up significant opportunities to advance our understanding of routes for turbostratic 2D graphite extraction, aimed at its use as a solid lubricant or as an additive for lubricant oils. The development of solid lubricants is proving to be a promising field of tribology, since they can aid with meeting the demands of energy efficiency through reducing the friction and wear. Their use as additives in lubricant oils is in accordance with the need to replace additives such as zinc dialkyl dithiophosphate (ZZDP) and molybdenum dithiocarbamate (MoDTC), due to environmental regulations that address concerns regarding the gas emissions of motor vehicles [18–21]. According to Spikes [19], these additives reduce the efficiency of catalysts and gas locking filters of the engine exhaust system and, therefore, vehicles fail to meet the gas emission regulations. For this reason, there is currently great interest in the identification and/or development of additives that could be substitutes for ZZDP and MoDTC, while also offering low sulphur, phosphorus and zinc levels [19,22,23].

Self-lubricating iron-based composites containing in situ generated turbostratic 2D graphite (TG) is one of the most promising choices for controlling friction and wear in modern energy-efficient systems [15].

In this study, powder metallurgy was used to obtain Fe-SiC composites in which the SiC particles were used as precursors to generate a large amount of turbostratic 2D graphite dispersed in the composite matrix [15]. Additionally, a method for chemical extraction using hydrofluoric acid [3] to isolate turbostratic 2D graphite nanoparticles from the metallic matrix is described. The structure and morphology of the extracted graphite were extensively examined by X rays diffractometry, Raman spectroscopy, and transmission electron microscopy. Particular emphasis is given to the feasibility of these particles as additives for lubricating oils. A turbostratic 2D graphite-based nanofluid was then chosen for transporting and supplying of solid lubricant agent to the contact area. Commercial 3D graphite-based nanofluids and pure POE oil were also tested for comparison. The tribological performance was investigated using incremental and constant load reciprocating sliding wear tests using a constant stroke (10 mm) and frequency (3 Hz). Experiments were conducted under controlled relative humidity ($50 \pm 6\%$) and temperature (22 ± 4 °C). The counter-body was a hard steel AISI 52100 ball (3 mm diameter), and a new surface area was used for each test. The same hard steel (AISI 52100) was used as a specimen. To impose a high-severity lubrication regime, the experiments were conducted under starved lubrication. In this regime, the severity of the contact is high due to the lack of hydrodynamic fluid film, i.e., the lubrication process is governed by the contact between the surfaces [24].

The scuffing resistance and friction coefficient values obtained in the lubricious regime of the incremental load tests are statistically equivalent regardless of the lubricant. However, the stability of both the scuffing resistance and the friction coefficient is higher for the tests conducted with the nanofluids.

The evolution of the friction coefficient with sliding distance in the constant load tests showed similar behaviour regardless of the lubricant. On the contrary, the time to achieve the steady-state regime, the maximum friction coefficient, and the average value of the

steady-state friction coefficient were higher for the tests conducted with pure oil as the lubricant. The DTG nanofluid induced the lowest wear rate of the specimens but did not show the best performance concerning the counter-bodies.

The wear mechanisms acting on the samples differed: In addition to evidence of abrasive wear predominantly on the edges of the wear scars, regardless of the lubricant, the tracks observed for tests using turbostratic 2D graphite-based nanofluid showed the predominance, particularly in the central part of the wear mark, of tribo-chemical wear, represented by the almost continuous presence of numerous islands of turbostratic 2D graphite-rich tribolayers. On the other hand, specimens used in tests with pure oil and commercial 3D graphite show detachments heterogeneously distributed throughout the central region. In the case of pure oil, small evenly distributed oxygen-rich tribolayer islands.

2. Materials and Methods

2.1. Synthesis, Extraction and Characterization of Turbostratic Graphite

Pure iron powder obtained from Höganäs do Brazil Ltda, Mogi das Cruzes, SP, Brazil (AHC 100.29) and SiC hexagonal powder (Micro Service-Micrograf 99501 UJ, Nacional de Grafite, São Paulo, SP, Brazil) with different particle sizes were used as raw materials. To obtain the largest amount of turbostratic 2D graphite, the selection of the alloy composition was established using a Fe-SiC phase diagram, generated in the Thermo-Calc[®] software (Computational tools for materials science, Version 2015b, database TCFE7 (Steel and Fe-alloys)) [25]. The selection of the alloy composition was established using the Fe-SiC phase diagram, generated in the Thermo-Calc software, in order to obtain the largest amount of turbostratic 2D graphite [25]. According to the phase diagram shown in Figure 1, the most favourable region for the formation of the largest amount of graphite lies between 1000 and 1150 °C with SiC contents of 17 to 19 wt.%. The alloy with 18.5 wt.% of SiC was chosen to evaluate the tribological performance of turbostratic 2D graphite particles, as indicated in Figure 1 [25].

The composite was prepared by mixing SiC and Fe powders with average particle sizes of 10 µm and 45 µm, respectively. The composite was homogenized in a Y-type mixer at 35 rpm for 45 min. After the mixing cycle, the alloy powder was fractionated in portions of 5 g. Compaction (600 MPa pressure) was performed in a double-action hydraulic press (Gabrielli L4). Each sample was produced in disk format with a diameter of 20 mm and weight of 5 g. The sintering was carried out in a resistive tubular furnace and the process parameters are presented in Table 1. The furnace was automatically turned off and cooled until room temperature at the end of the cycle. The gas flow was interrupted at 200 °C, and the samples were removed when the furnace temperature was below 80 °C. All samples were sintered at 1150 °C. In addition, a well-known method for chemical extraction using hydrofluoric acid (HF) to isolate the turbostratic 2D graphite nanoparticles from the metallic matrix was used, Figure 2a [25]. Briefly, after sintering, the samples were fragmented into small pieces using a side cutter. The fragments were then placed in a plastic vessel containing 100 mL of HF. The chemical reaction occurred under stirring for 2 h, followed by double washing in distilled water. Subsequently, the powder was soaked in 100 mL of absolute ethyl alcohol and then dried on a heating plate (150 °C for 1 h). At the end of the chemical extraction, the mass of the extracted powder was measured. This process was repeated until the stoichiometric mass of graphite was reached.

Table 1. Sintering parameters.

Sintering Parameters	
Temperature	1150 °C
Gas composition	95% Ar + 5% H ₂
Heating rate	10 °C/min
Time	1 h

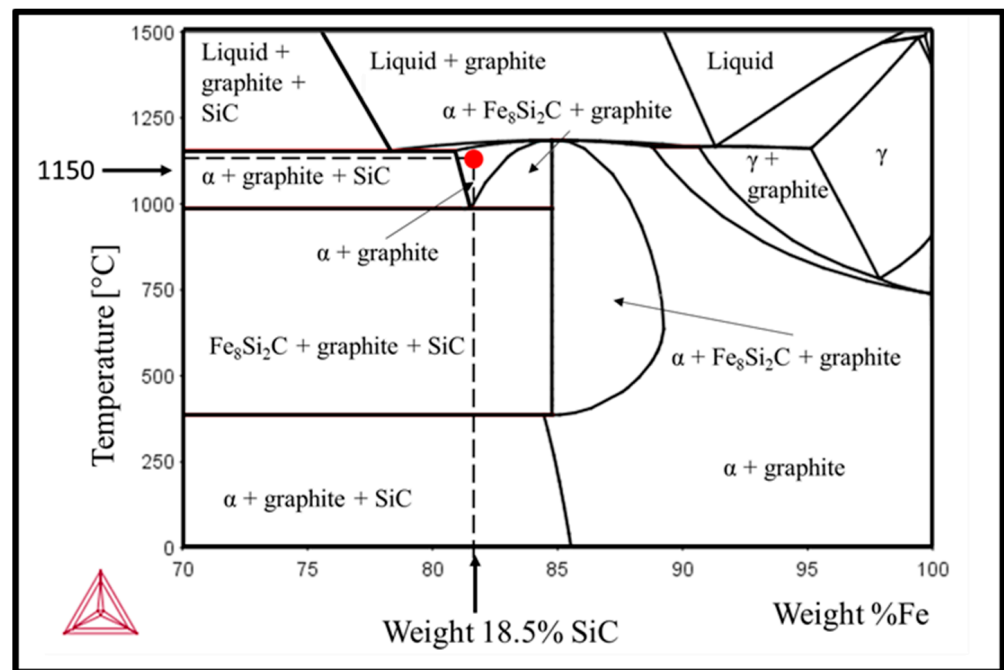


Figure 1. Fe-SiC phase diagram generated by the Thermo-Calc[®] software. The red point indicates the composition and sintering temperature of the alloy studied.

Phase analysis was carried out on all samples using a Philips X'Pert diffractometer (Netherlands). The diffractograms were recorded using $\text{CuK}\alpha$ ($\lambda = 1.5418 \text{ \AA}$) radiation and employing the Bragg-Brentano geometry ($0^\circ \leq 2\theta \leq 120^\circ$; 0.05° angular step; 2 s step time; 40 kV and 30 mA). The Inorganic Crystal Structure Database (ICSD) database was used to identify the phases.

Raman spectroscopy analysis was performed at a wavelength of 514.5 nm argon laser on a Renishaw In Via spectrometer (UK) Five ($2 \mu\text{m}^2$) regions were selected with the aid of an optical microscope. In each region, five acquisitions were performed in the range of $1000\text{--}3400 \text{ cm}^{-1}$. An average of 25 acquisitions comprised the characteristic Raman spectrum of each sample. TEM analysis was performed using a JEOL (JEM-1000, Tokyo, Japan) microscope operating at 100 kV. Bright-field (BF) and selected area electron diffraction (SAED) patterns were obtained with a Gatan charge-coupled device (CCD) camera. The samples for TEM analysis were prepared as follows: carbon flakes (or sheets) resulting from the chemical extraction procedure were placed in an ultrasonic bath with ethanol solution for a few minutes. In the next step the solution was dripped onto a copper grid and then dried in ambient air. The corresponding d values of the diffraction rings were measured with the Diffpack digital micrograph program (Gatan, Inc., Pleasanton, CA, USA).

2.2. Tribological Evaluation

The tribological performance was investigated using incremental and constant load reciprocating sliding wear tests. To impose a high-severity lubrication regime, the experiments were conducted under starved lubrication.

2.2.1. Preparation of Turbostratic 2D Graphite-Based Nanofluids

Turbostratic 2D graphite particles were dispersed (1:100 mass ratio) in pure mineral oil (apolar, 0.8491 g/cm^3 , 11.85 cSt at 40°C) to act as a lubricant additive (dispersion of turbostratic graphite—DTG). A commercial graphite (Nacional Graphite—Micrograf 99501 UJ; 99.95% C; $d_{50} = 0.83 \mu\text{m}$) (dispersion of commercial graphite—DCG) and pure oil were also tested for comparison. The dispersions were prepared in two steps, as illustrated in Figure 2b. In the first step, the mineral oil was functionalized using oleic acid to stabilize

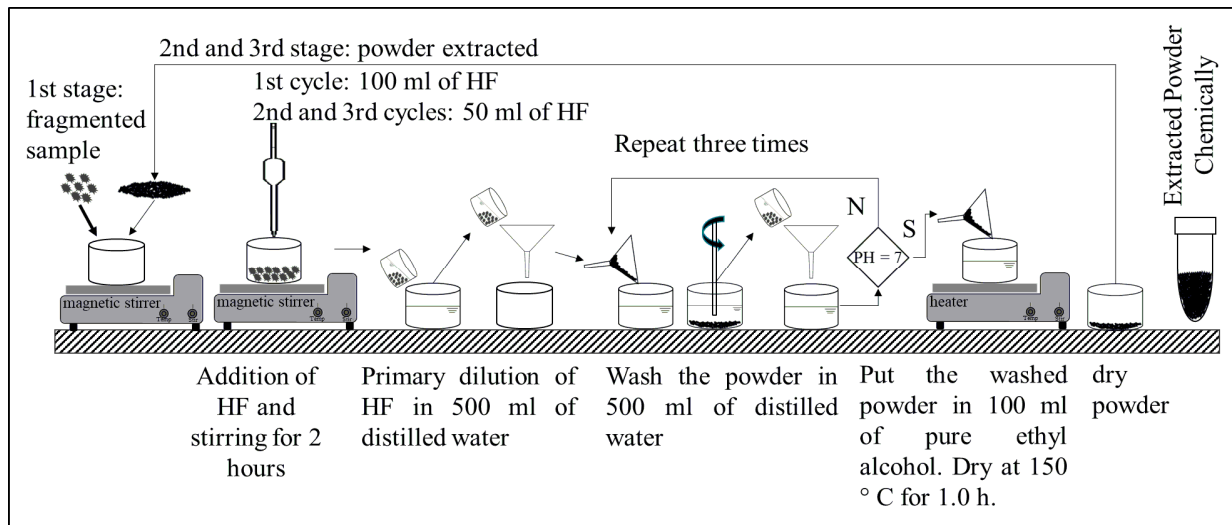
the dispersed particles owing to steric repulsion. The functionalization of the mineral oil involves the emulsification of the dispersant (oleic acid) in the solvent (mineral oil). Thus, 3 mg of oleic acid was added to the mineral oil under stirring for 1 h. After this time, 300 mg of turbostratic 2D graphite particles was added to the functionalized oil and the mixture was kept under stirring for 24 h. In the second step, an ultrasonic sonicator was used to exfoliate and dispersed turbostratic 2D graphite particles in the pure mineral oil (PMO) employing three cycles of sonication of 1 min each. After sonication, a Zetasizer Nano ZS (Red Badge) analyser, model ZEN3600 (Malvern Instruments, Great Malvern, UK), was used to determine the hydrodynamic diameter of the particles, i.e., the average size of the nanoparticle clusters present in the nanofluids. In the Zetasizer Nano analyser, the principle of dynamic light scattering (He-Ne laser, wavelength $\lambda = 633$ nm/red and maximum power of 5 mV) was used to determine the hydrodynamic diameter of the nanoparticles. This equipment can measure the hydrodynamic diameter of particles in a size range of 0.3 nm to 10 μm . After each cycle in the sonicator, a fraction of 10 μL was removed from the lubricant dispersion and diluted in a vial with 1.5 mL of mineral oil to perform the test. The dilution was necessary because for the characterization of the particle size distribution due to the turbidity of the dispersion.

The dispersion of a commercial graphite (DCG), used as a reference, was then prepared using the same procedure described for the DTG.

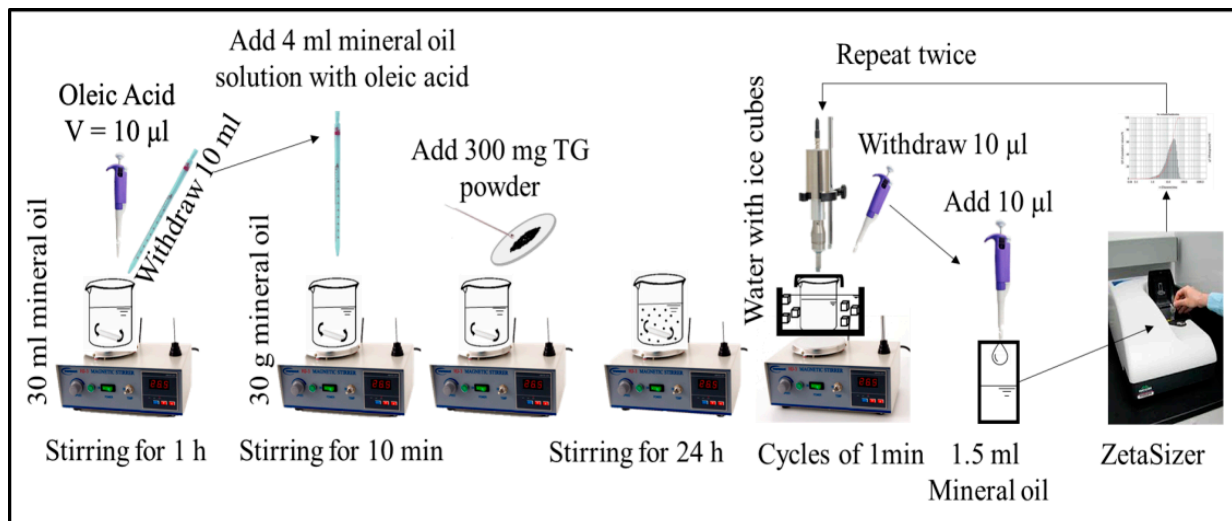
2.2.2. Tribological Characterization

The tribological characterization was performed with a Bruker, CETR UMT, USA, tribometer using constant starved lubrication and incremental load reciprocating sliding tests with a constant stroke (10 mm) and frequency (3 Hz). Experiments were conducted under controlled relative humidity ($50 \pm 6\%$) and temperature (22 ± 4 °C). The counter-body was a hard steel AISI 52100 ball (3 mm diameter), and a new surface area was used for each test. The same hard steel (AISI 52100) was used as a specimen. For this, the samples were cut to the appropriate dimensions, and polished to a mirror-like surface ($S_q = 0.123 \pm 0.089$ μm ; $S_{ku} = 31.22 \pm 19.8$ and $S_{sk} = -3.012 \pm 1.04$) using conventional metallographic techniques. The incremental load tests started at a load of 50 N and the methodology proposed by De Mello and Binder [4] was applied, with increments of 25 N at 10 min intervals to determine the scuffing resistance. In this paper, the scuffing resistance is specified as the work (N.m) until the friction coefficient exceeded the value of 0.2 and remained above this limit for at least 190 s. This point is essential to avoid premature interruption of the test due to fluctuations in the friction coefficient, which may occur during increases in the normal load. In the constant load tests, a constant normal load of 300 N was used for 1 h to obtain the friction coefficients and wear rates of the specimens and counter-bodies. For each condition, at least five measurements were performed.

White light interferometry (ZygoNewView 7300, New York, USA) was used to quantify the specimen wear volumes. Axonometric projections of the wear marks (Figure 6) were obtained and from these the volumetric variation was calculated using MountainsMap Universal 7.1[®] software. After levelling, an average profile was obtained, and the volumetric wear was quantified by the area corresponding to the wear track (Figure 6) multiplied by the wear mark length. The wear rate of the counter-bodies was obtained by measuring the cap diameter formed in the sphere. This measurement was performed with the aid of an optical microscope coupled with an image analyser. From the value of this diameter, the volume of material removed, and the wear rate were calculated as previously reported [26]. Wear scars were analysed using a scanning electron microscope (VEGA3 LM, Tescan, Czech Republic), white light interferometry (Zygo NewView 7300) and Raman spectrometry. Raman analysis was conducted at a wavelength of 514.5 nm using an Ar laser Renishaw inVia system. In each case, results reported are the average of at least five tests conducted under identical experimental conditions.



(a)



(b)

Figure 2. Schematic showing the processing steps. (a) HF-based purification process. (b) involved in the nanofluid preparation.

3. Results and Discussion

3.1. Characterization of Extracted Particles

The X-ray diffraction (XRD) pattern shown in Figure 3a reveals that the powder extracted from sintered samples is mono-phase, and it was identified and indexed as graphite according to standard charts (ICSD 52230). Figure 3b shows the Raman spectrum (RS) of the extracted powder, which is characteristic of graphite material. The presence of the D band associated with crystalline disorder can be noted. The ID/IG ratio (0.09 ± 0.02) and the crystallite size ($500.35 \pm 32.13 \text{ \AA}$) are, according to the literature [27–30], strong evidence of disorder in the material. The full-width at half-maximum ($\text{FWHM} = 69.16 \pm 3.37$) and the conical shape of the second-order G' band are consistent with two-dimensional graphite, also called turbostratic 2D graphite.

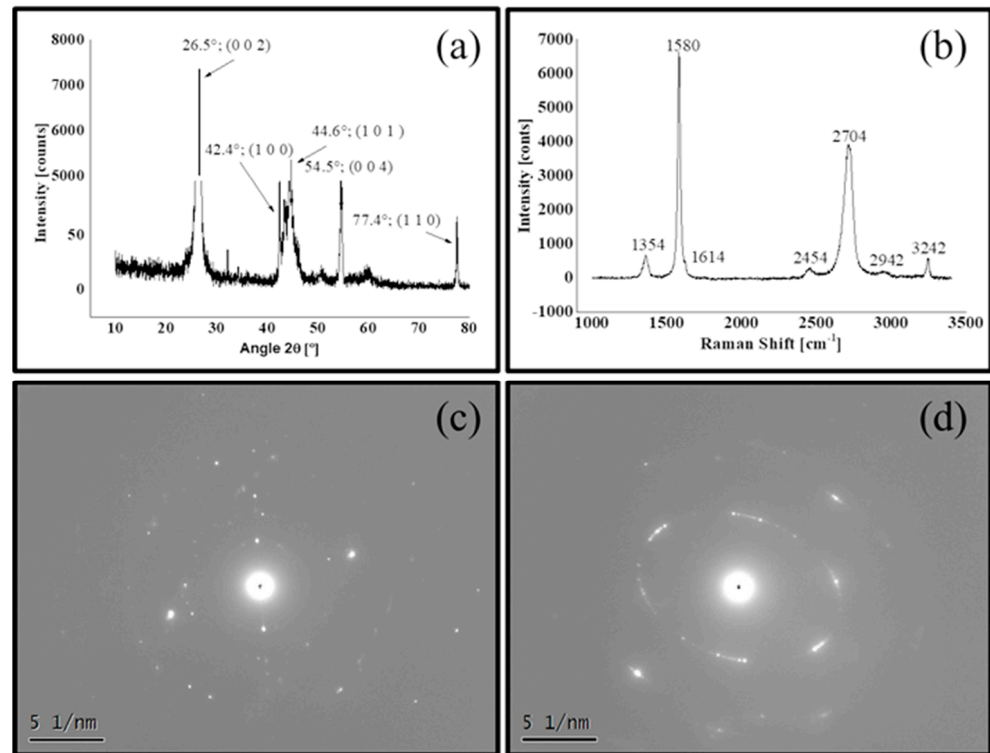


Figure 3. Characterization of turbostratic graphite powder: (a) X-ray diffraction—indexed as graphite by standard charts ICSD 52230; (b) Raman spectrum; (c) the SAED pattern showing the basal plane (002); and (d) the SAED pattern showing elliptical rings typical of disordered structures.

The selected area electron diffraction (SAED) pattern shown in Figure 3c was indexed as (002), (100), (101), (004), and (110) planes, confirming the presence of a polycrystalline material with a $P6/mmc$ hexagonal symmetry. This indexing is in agreement with the X-ray diffraction results. The measured interplanar distance of the (002) basal plane was approximately 3.41 Å. This is larger than the interplanar distance along the c -axis of a typical graphite structure (~ 3.34 Å). However, it is similar to that of the disordered form, which is known as turbostratic graphite [2,29]. Other evidence that indicates turbostratic characteristics is the elliptical rings shown in Figure 3d [31–35].

Figure 4 shows the distribution of the hydrodynamic diameters of the nanofluids. The turbostratic graphite nanofluid (DTG) shows a bimodal distribution in the lubricant dispersions, with modes of 1.720 and 3.090 nm. In the case of the dispersion of commercially available graphite (DCG), the hydrodynamic diameter distribution is also bimodal, with modes of 396 and 615 nm, i.e., smaller clusters compared with DTG. The bimodal distribution is likely due to the aggregation of particles not disaggregated by the ultrasonic sonicator. The bimodal distribution is likely due to the agglomeration of particles not disaggregated by the ultrasonic sonicator.

3.2. Tribological Characterization

3.2.1. Incremental Load Tests

Figure 6 reports the main results obtained in the incremental load tests. The bars represent the average values of the scuffing resistance, while the triangles show the average values for the friction coefficient (FC) in the lubricious regime ($\mu < 0.2$). These values were found to be statistically equivalent (ANOVA). However, the stability of both the scuffing resistance and, to a lesser extent, of the friction coefficient is higher for nanofluids, in particular for the DCG, as indicated by the dispersion bars of the results. For DCG tests, all the runs reached the limit of the load cell of the tribometer (500 N). In this sense, as all load averages were the same, the variability was zero.

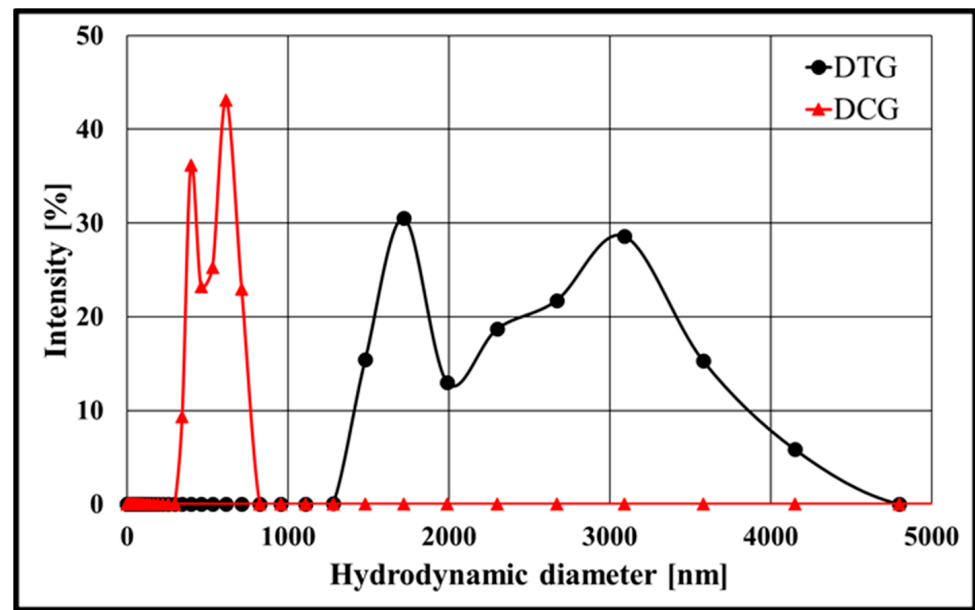


Figure 4. Distribution of hydrodynamic diameter of nanofluids.

3.2.2. Constant Load Tests

Figure 5 shows typical aspects of the central region of the wear scars and the average profile of the cross-sections of the specimens. It is possible to perceive the presence of more than one wear mechanism: abrasion, acting mainly on the edges of the wear marks (arrows), and adhesive and tribochemical wear in the inner part of the track. The prevalence of these mechanisms varies according to the lubricant. Analysis of the average cross-sectional profiles reveals the higher wear intensity of the samples related to the tests where lubrication was carried out with pure oil and commercial-based graphite nanofluid. In the tests where lubrication was performed with the turbostratic graphite-based nanofluid, the samples showed the lowest worn volume $4.99 \times 10^{-3} \pm 0.698 \times 10^{-3} \text{ mm}^3$ versus $7.21 \times 10^{-3} \pm 1.26 \times 10^{-3} \text{ mm}^3$ and $10.00 \times 10^{-3} \pm 2.42 \times 10^{-3} \text{ mm}^3$ for lubrication with pure oil and commercial graphite-based nanofluid, respectively.

Figure 7a shows the evolution of the friction coefficient with sliding distance in the constant load tests. The evolution can be divided into two regimes: running-in and steady-state. The running-in regime, shown in Figure 7b, can be characterized by a sliding distance in which the tribological system adjusts to the operating parameters until a steady-state regime is established (Figure 7c) [36].

The progress of the friction coefficient in the running-in regime shown in Figure 7b is different in the tests with the DTG when compared to DCG. In the DCG tests, it reaches the maximum value (0.184) within a very short sliding distance (0.47 m) and decays progressively to the steady-state value (0.080) in about 3.90 m. In the DTG tests, the maximum friction coefficient (0.214) is reached at a distance of 3.71 m and decays to the steady-state value (0.073) at a distance of 7.1 m. This difference in behaviour may be associated with the hydrodynamic diameter distribution of the two nanofluids determined at the beginning of the tests.

It is reasonable to assume that, due to the smaller hydrodynamic diameter (Figure 4), the commercial graphite aggregates penetrate more easily, making contact and subsequently providing immediate protective action. In contrast, given the larger size of the turbostratic graphite aggregates it is difficult for them to make contact, delaying their effective action. For this reason, both the maximum friction coefficient and the sliding distance to achieve the running-in regime in the DTG nanofluid tests were practically twice the corresponding values observed in the DCG tests. Although this hypothesis needs to be confirmed by further studies, the same effect was found by Bordignon et al. [37], studying

the influence of plasma functionalization of multilayer graphene (MG) as an additive for low-viscosity polyol ester oil. Pure MG and MG functionalized via N₂, and NH₃ plasma were analysed. They observe that in the POE + MG samples, the MG agglomeration leads to a less stable suspension (large clusters), preventing the nanoparticles from entering the sliding contact and allowing metal-metal contact. However, the addition of MG-NH₃ in POE oil provides a well-dispersed suspension (small clusters), which contributes to forming a continuous and homogeneous anti-wear tribofilm between the rubbing surfaces.

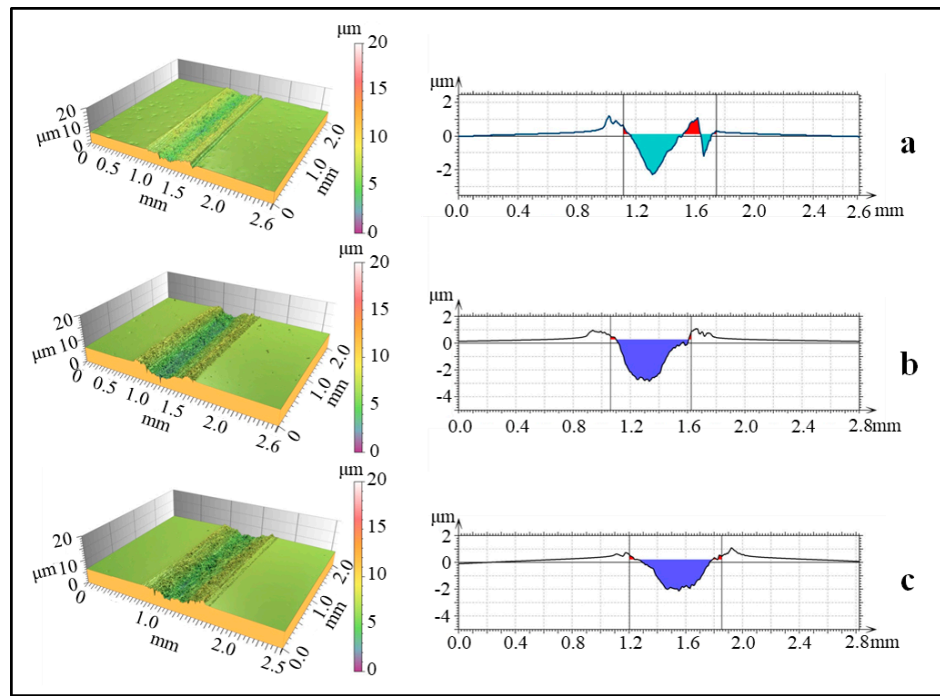


Figure 5. Typical aspects and average profile of the wear scars obtained by white light interferometry. (a) DTG. (b) Pure oil. (c) DCG.

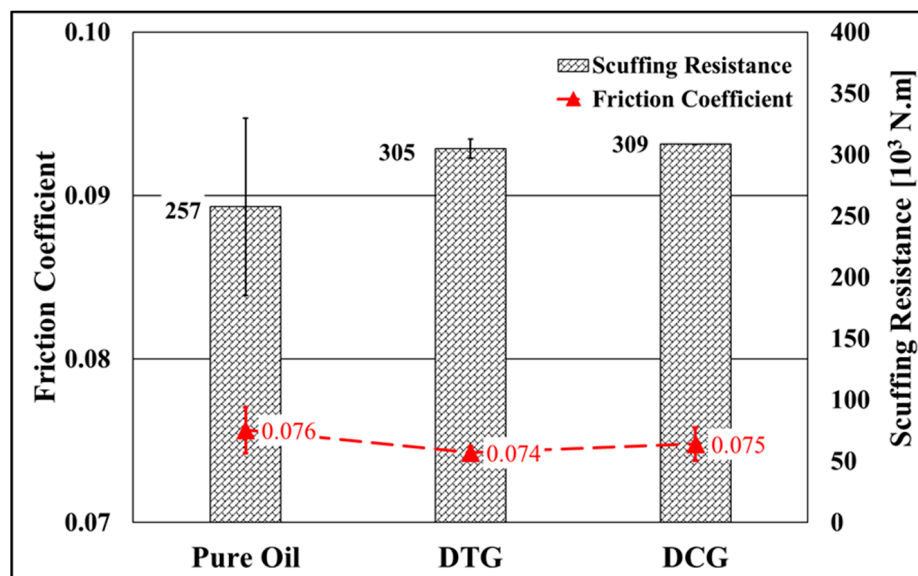


Figure 6. Incremental load tests.

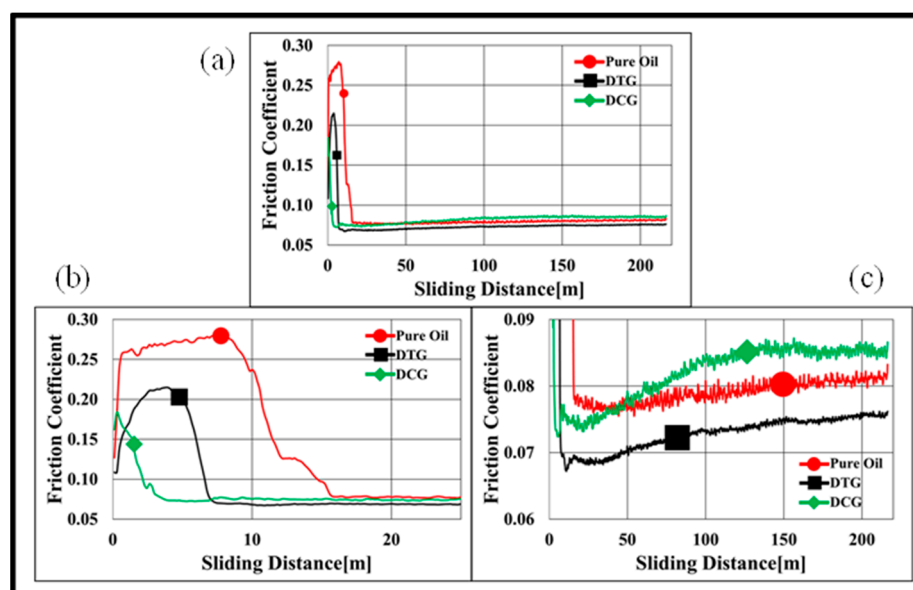


Figure 7. Evolution of friction coefficient with sliding distance: (a) full evolution, (b) running-in regime and (c) steady-state regime.

To gain a better understanding of this behaviour, additional tests were performed and interrupted at the end of the running-in period. The wear scars were then analysed by white light interferometry. Analysis of the cross-sections obtained in the tests (Figure 8) revealed that plastic deformation plays a predominant role in the formation of the wear marks. The volume loss associated with commercial graphite-based nanofluids was low, as seen in Figure 8a, since 86% of the total volume of the groove piled up at the edge of the wear scars. On the other hand, in the tests with the turbostratic graphite-based nanofluid (Figure 8b) only 58% of the groove volume stacked up at the edges, i.e., 42% was transformed into wear debris, probably contributing to the formation of a 2D turbostratic graphite-rich third body in the DTG experiments, as evidenced by the lower average friction coefficient throughout the steady-state in the tests using DTG as an additive (Figure 7c).

The tendency toward smaller clearances and increased speeds imposes high wear resistance on the tribological pair [5]. In this regard, the wear of both specimens and counter-bodies is essential in systems operating under severe conditions. The use of carbon-based nanoparticles as lubricant oil additives reduces the wear rate of the tribological system (Figure 9). The DTG nanofluid induced the lowest wear rate of the specimens but did not show the best performance concerning the counter-bodies. The reductions in the average wear rate for specimen and counter-body were 26% and 47%, respectively, in the DTG tests compared to the pure oil tests, evidencing an excellent performance of turbostratic 2D graphite nanoparticles as a lubricant additive. However, the comparison between the wear rates obtained in the tests with DTG and DCG nanofluids presented an unexpected result, that is, the wear rate of the counter-body in the DCG tests was lower compared to the tests performed with the DTG-based nanofluid, which may be associated with the combined effect of hydrodynamic diameter distribution and wear mechanisms.

Figure 10 presents an overview of the sample wear scars and the difference in the wear mechanisms is clear. The track for tests using turbostratic 2D graphite-based nanofluid, seen in Figure 10a, shows evidence of abrasive wear at the edges and a predominance, particularly in the central part of the wear mark, of tribochemical wear, represented by the almost continuous numerous islands of tribolayers. On the other hand, the images obtained for tests with commercial 3D graphite in Figure 10b and pure oil in Figure 10c show evidence of abrasive wear associated with detachments heterogeneously distributed throughout the central region, and, in the latter case, small, evenly distributed tribolayer islands.

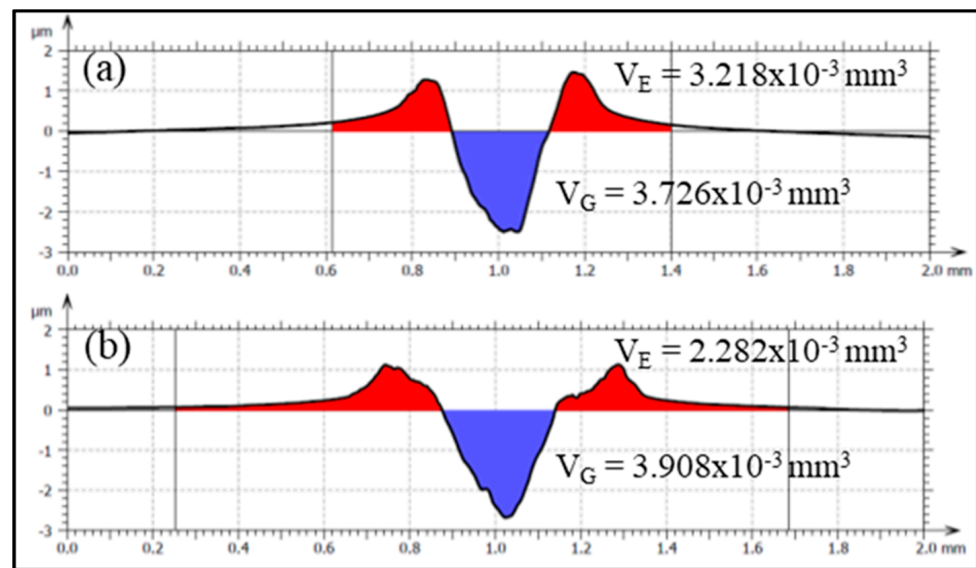


Figure 8. Cross-section of the typical average wear scar in the interrupted tests: (a) DCG and (b) DTG.

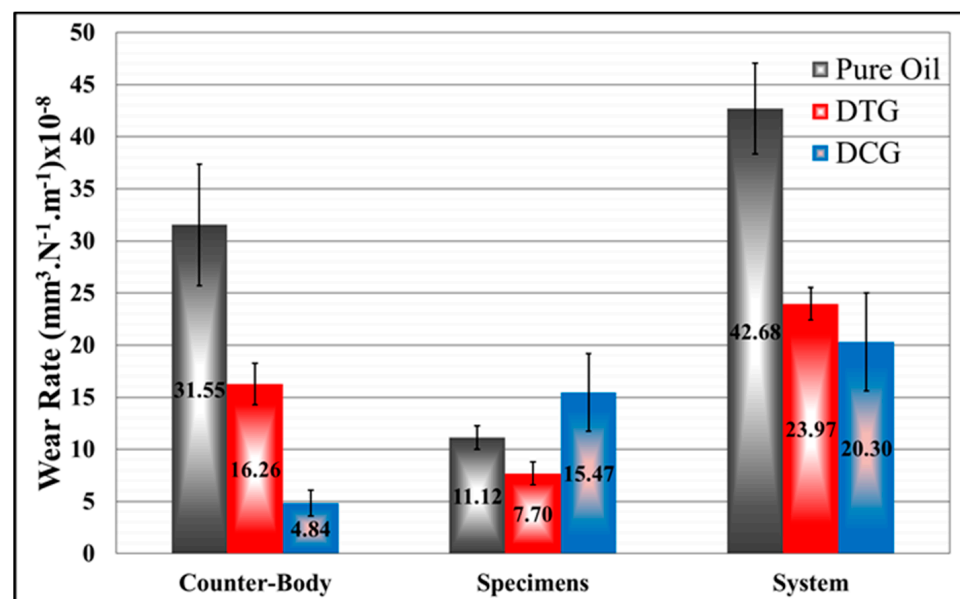


Figure 9. Average wear rate.

Figure 11 illustrates the typical wear mechanism presented by the samples submitted to the test using the turbostratic 2D graphite-based nanofluid. In addition to the grooves typically associated with abrasive wear present at the wear scar edge, the formation of tribolayers islands homogeneously distributed in the central part predominates. The insert in Figure 11 shows one of these islands. The analysis by EDX (Figure 11d) showed that they are mostly made up of iron, oxygen and carbon, the latter in turbostratic form as illustrated by the Raman spectrum in Figure 11c. It is reasonable to assume that the excellent tribological performance imparted by the turbostratic graphite-based nanofluid is due to the high mechanical strength tribolayer formed by the tribochemical reactions between the wear debris from both specimens and counter-bodies and the solid lubricating particles of the turbostratic graphite dispersion.

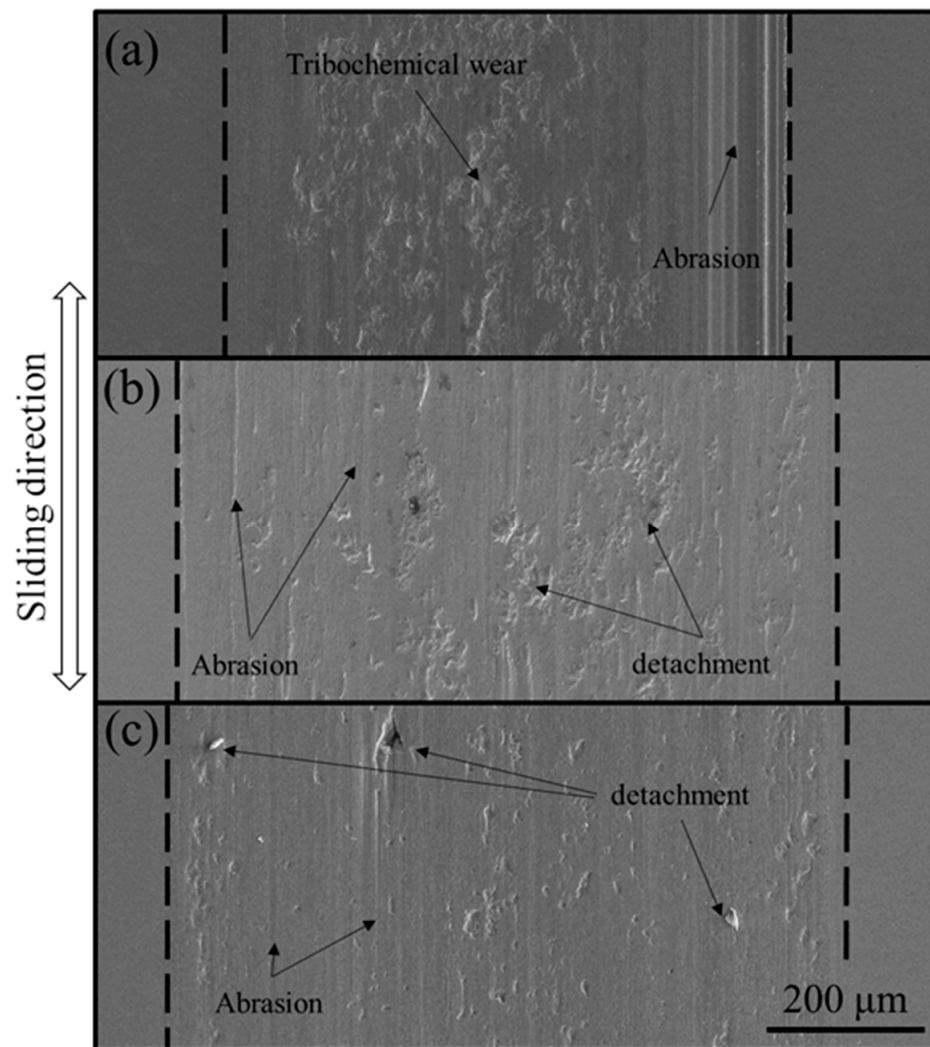


Figure 10. Overview of wear marks showing typical wear mechanisms: (a) DTG, (b) DCG and (c) pure oil.

In fact, the similarity between the Raman spectra obtained for the tribolayer islands in the central parts of the wear mark, seen in Figure 11c, and the powdered turbostratic graphite used as an additive (Figure 3b) indicates that the turbostraticity is maintained even after the tribological phenomenon, a factor also noted in the literature [2,3,5,15,17] as the origin of the excellent tribological performance. All of these characteristics are compatible with the tribochemical wear mechanism [23]. The formation of iron oxide was also observed in the smooth regions, free of tribolayers (position 'b' in the insert of Figure 11) as illustrated by the Raman spectrum in Figure 11b.

As shown in Figure 10b, the wear mechanism for the samples of the tests using commercial graphite-based nanofluid is characterized by intense material detachment. In some regions within the wear scars (Figure 12a), a tenuous tribolayer comprised of iron oxides and graphite was observed, as indicated by the associated Raman spectrum in Figure 12a. In other regions (Figure 12b), black islands are clearly visible and these are mainly composed of carbon, as indicated by the EDX analysis.

The most significant difference presented by the wear mechanism associated with the tests with pure oil as the lubricant, as previously noted, was the presence of small, evenly distributed tribolayer islands, shown in the insert of Figure 13, which are rich in oxygen, as verified in the associated EDX analysis (Figure 13b.1). The Raman spectrum (Figure 13b.2) of the region shows, in addition to the presence of oxides (bands at low frequencies), bands

characteristic of disordered carbonaceous materials, probably a consequence of the reaction of the lubricating oil during the tribological phenomenon.

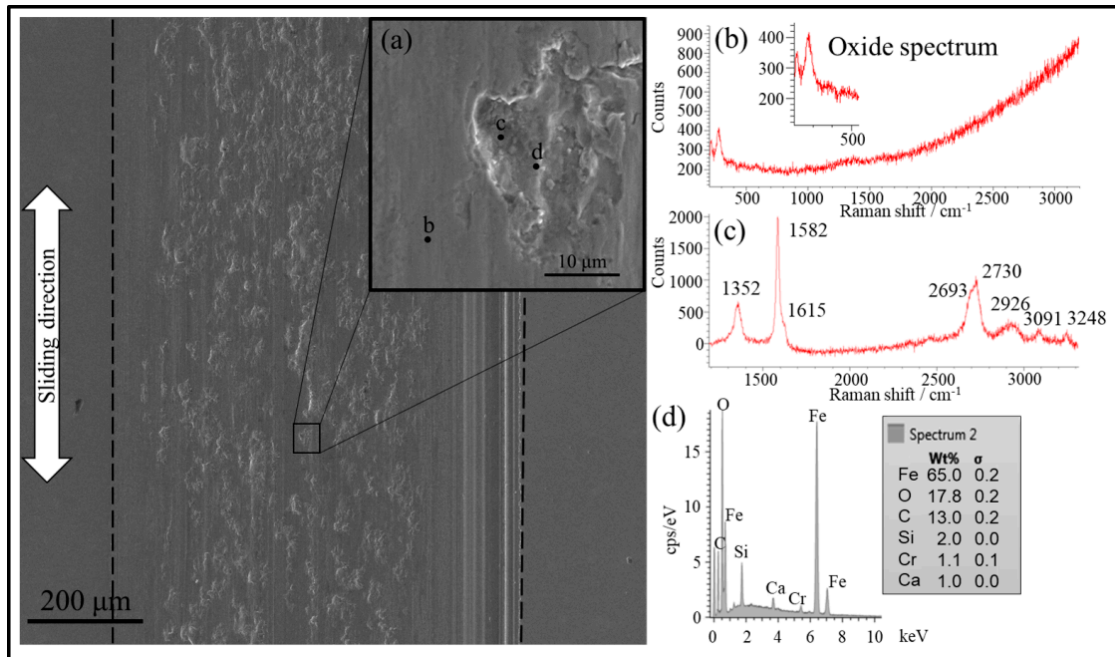


Figure 11. Typical wear scar analysis of turbostratic 2D graphite-based nanofluid. Raman spectra (b,c) taken at positions 'b' and 'c' indicated in the insert (a,d) EDX results.

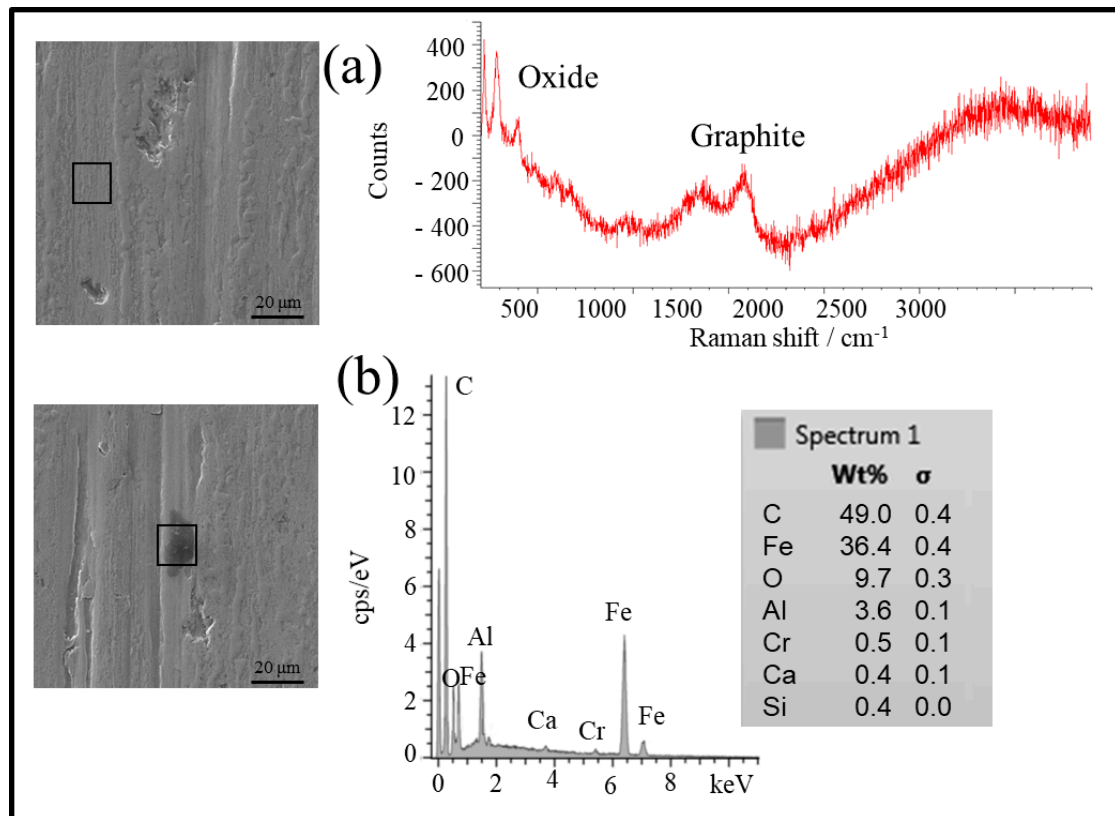


Figure 12. Typical wear aspects and chemical characterization (Raman spectroscopy and EDX analysis) in different regions within the specimen wear mark (test with commercial graphite-based nanofluid).

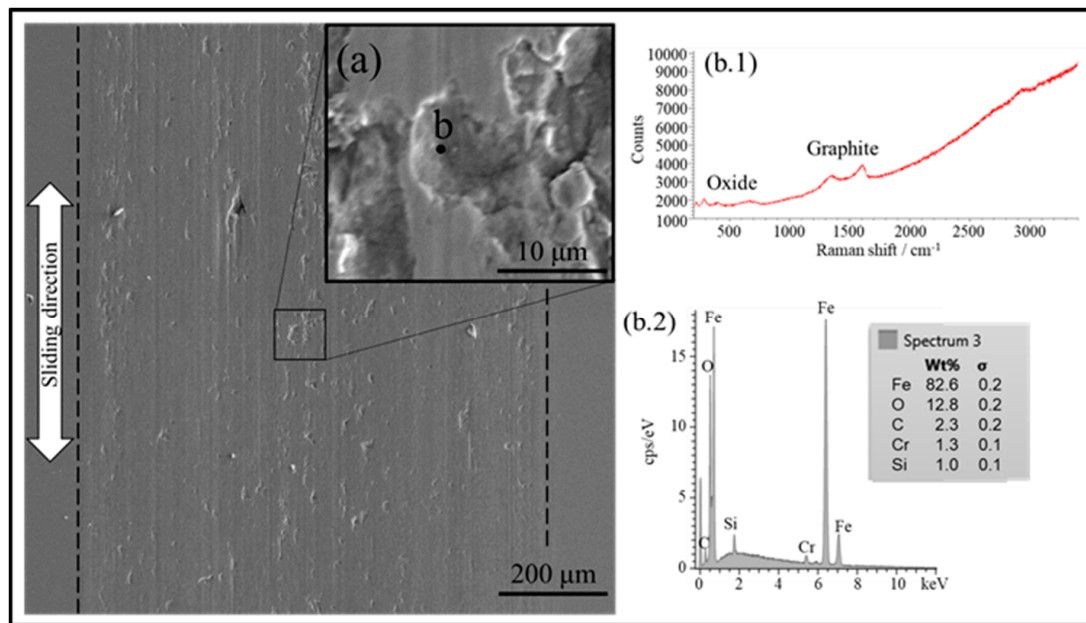


Figure 13. Analysis of typical wear scar produced during the test with pure oil as the lubricant. Raman spectra (b.1) and the EDX results (b.2) indicated in point 'b' of the insert (a).

4. Conclusions

In this study, powder technology was used to obtain Fe-SiC composites in which SiC particles act as precursors to generate a large amount of turbostratic 2D graphite dispersed in the composite matrix. The chemically extracted turbostratic 2D graphite was used as an additive for mineral oil. Commercial graphite-based nanofluids and pure oil were also tested for comparison. The main results can be summarized as follows:

1. The powder obtained was analysed (XRD, Raman spectroscopy, SEM, and TEM) and characterized as turbostratic 2D graphite;
2. The hydrodynamic diameter distribution of the turbostratic 2D graphite-based nanofluid shows a bimodal distribution with modes of 1.720 and 3.090 nm;
3. The values for the scuffing resistance and friction coefficient obtained in the lubricious regime of the incremental load tests are statistically equivalent regardless of the lubricant. However, the stability of both the scuffing resistance and, to a lesser extent, of the friction coefficient is higher for the tests conducted with the nanofluids;
4. The evolution of the friction coefficient with sliding distance in the constant load tests showed similar behaviour regardless of the lubricant, that is, a maximum followed by a progressive decay to the steady-state value. However, the time to achieve the steady-state regime, the maximum friction coefficient, and the average value of the steady-state friction coefficient varied, being higher for the tests conducted with pure oil as the lubricant. For nanofluids, these parameters could be associated with the hydrodynamic diameter distribution at the beginning of the tests: a smaller hydrodynamic diameter (DCG) induced shorter times and lower friction coefficient maximum but higher friction coefficient;
5. The use of carbon-based nanoparticles as a lubricant oil additive reduces the wear rate of the tribological system. The DTG nanofluid induced the lowest wear rate of the specimens but did not show the best performance concerning the counter-bodies. The reductions in the average wear rate for the specimens and counter-body were 26% and 47%, respectively, in the DTG tests compared to the pure oil tests. This demonstrates the excellent performance of turbostratic 2D graphite nanoparticles as a lubricant additive; and
6. The wear mechanisms acting on the samples differed: the tracks observed for tests using turbostratic 2D graphite-based nanofluid provide evidence of abrasive wear

on their edges and the predominance, particularly in the central part of the wear mark, of tribo-chemical wear, represented by the almost continuous presence of numerous islands of turbostratic 2D graphite-rich tribolayers. On the other hand, specimens used in tests with pure oil and commercial 3D graphite show evidence of abrasive wear associated with detachments heterogeneously distributed throughout the central region and, in the case of pure oil, small evenly distributed oxygen-rich tribolayer islands.

5. Patents

Neves, G.O.; Rivera, N.I.A.; Klein, A.N.; Binder, C.; Dias, H.W.J.; Pereira, R.V.; Rodrigues Neto, J.B.; Mello, J.D.B.; Binder, R. Método para Produção de Partículas de Carbono Nanoestruturado Através de Reações no Estado Sólido entre Materiais Inorgânicos Particulados. BR Patent 1,020,200,007,483, 11 June 2020.

Author Contributions: Conceptualization, A.N.K., J.B.R.N., C.B. and J.D.B.d.M.; methodology, J.B.R.N. and J.D.B.d.M.; formal analysis, J.B.R.N., C.B. and J.D.B.d.M.; investigation, A.B.M. and H.W.J.D.; resources, C.B.; writing—original draft preparation, H.W.J.D.; writing—review and editing, J.D.B.d.M.; supervision, J.B.R.N. and J.D.B.d.M.; project administration, C.B. and A.N.K.; funding acquisition, C.B. and A.N.K. All authors have read and agreed to the published version of the manuscript.

Funding: This research was funded by Brazilian Development Bank (BNDES), grant number 14.2.0220.1 (2014–2017).

Acknowledgments: The authors acknowledge the Brazilian Development Bank (BNDES), as well as Whirlpool/Embraco, for funding this research program and for technical contributions.

Conflicts of Interest: The authors declare no conflict of interest.

References

1. Binder, C.; Hammes, G.; Schroeder, R.; Klein, A.N.; de Mello, J.D.B.; Binder, R. “Fine tuned” steels point the way to a focused future. *Metal Powder Rep.* **2010**, *65*, 29–37. [[CrossRef](#)]
2. de Mello, J.D.B.; Binder, C.; Binder, R.; Klein, A.N. Effect of precursor content and sintering temperature on the scuffing resistance of sintered self lubricating steel. *Wear* **2011**, *271*, 1862–1867. [[CrossRef](#)]
3. De Mello, J.D.B.; Binder, C.; Hammes, G.; Klein, A.N. Effect of the metallic matrix on the sliding wear of plasma assisted debinded and sintered MIM self-lubricating steel. *Wear* **2013**, *301*, 648–655. [[CrossRef](#)]
4. de Mello, J.D.B.; Binder, R. A methodology to determine surface durability in multifunctional coatings applied to soft substrates. *Tribol. Int.* **2006**, *39*, 769–773. [[CrossRef](#)]
5. Binder, C.; Bendo, T.; Pereira, R.V.; Hammes, G.; De Mello, J.D.B.; Klein, A.N. Influence of the SiC content and sintering temperature on the microstructure, mechanical properties and friction behaviour of sintered self-lubricating composites. *Powder Metal* **2016**, *59*, 384–393. [[CrossRef](#)]
6. Donnet, C.; Erdemir, A. Historical developments and new trends in tribological and solid lubricant coatings. *Surf. Coat. Int.* **2004**, *180–181*, 76–84. [[CrossRef](#)]
7. Erdemir, A. Review of engineered tribological interfaces for improved boundary lubrication. *Tribol. Int.* **2005**, *38*, 249–256. [[CrossRef](#)]
8. Kato, H.; Takama, M.; Iwai, Y.; Washida, K.; Sasaki, Y. Wear and mechanical properties of sintered copper–tin composites containing graphite or molybdenum disulfide. *Wear* **2003**, *255*, 573–578. [[CrossRef](#)]
9. Erdemir, A. Chapter 22: Solid Lubricants and Self-Lubricating Films. In *Modern Tribology Handbook II*; Bhushan, B., Ed.; CRC Press: Boca Raton, FL, USA, 2001; pp. 787–825.
10. Tascón, J.M.D. Materiales de carbono: Estructuras y formas (Carbon materials: Their structures and types). *Opt. Pura Apl.* **2007**, *40*, 149–159.
11. Dresselhaus, M.S. Future Directions in Carbon Science. *Annu. Rev. Mater. Res.* **1997**, *27*, 1–34. [[CrossRef](#)]
12. Kumar, N.; Pandian, R.; Das, P.K.; Ravindran, T.R.; Dash, S. High-temperature phase transformation and low friction behaviour in highly disordered turbostratic graphite. *J. Phys. D Appl. Phys.* **2013**, *46*, 1–10. [[CrossRef](#)]
13. Tuinstra, F.; Koenig, J.L. Raman Spectrum of Graphite. *J. Chem. Phys.* **1970**, *53*, 1126–1130. [[CrossRef](#)]
14. Klein, A.N.; Furlan, K.P.; Schroeder, R.M.; Hammes, G.; Binder, C.; Neto, J.B.R.; Probst, S.H.; de Mello, J.D.B. Thermodynamic aspects during the processing of sintered materials. *Powder Technol.* **2015**, *271*, 193–203. [[CrossRef](#)]

15. Binder, C. Desenvolvimento de novos Tipos de aços Sinterizados Autolubrificantes a seco com Elevada Resistência Mecânica Aliada a Baixo Coeficiente de Atrito via Moldagem de pós por Injeção. Ph.D. Thesis, Universidade Federal de Santa Catarina, Florianópolis, Brazil, 2009; 170p. (In Portuguese)
16. Consoni, D.R. Morfologia e Estrutura dos Nódulos de Grafite Gerados pela Dissociação de SiC na Sinterização. Ph.D. Thesis, Universidade Federal de Santa Catarina, Florianópolis, Brazil, 2014; 155p. (In Portuguese)
17. Binder, C.; Bendo, T.; Hammes, G.; Neves, G.; Binder, R.; de Mello, J.; Klein, A. Structure and properties of in situ-generated two-dimensional turbostratic graphite nodules. *Carbon* **2017**, *124*, 685–692. [[CrossRef](#)]
18. Williamson, W.; Perry, J.; Gandhi, H.; Bombach, J. Effects of oil phosphorus on deactivation of monolithic three-way catalysts. *Appl. Catal.* **1985**, *15*, 277–292. [[CrossRef](#)]
19. Spikes, H. Low- and zero-sulphated ash, phosphorus and sulphur anti-wear additives for engine oils. *Lubr. Sci.* **2008**, *20*, 103–136. [[CrossRef](#)]
20. Greenall, A.; Neville, A.; Morina, A.; Sutton, M. Investigation of the interactions between a novel, organic anti-wear additive, ZDDP and overbased calcium sulphonate. *Tribol. Int.* **2012**, *46*, 52–61. [[CrossRef](#)]
21. Parsaeian, P.; Ghanbarzadeh, A.; Van Eijk, M.C.; Nedelcu, I.; Neville, A.; Morina, A. A new insight into the interfacial mechanisms of the tribofilm formed by zinc dialkyl dithiophosphate. *Appl. Surf. Sci.* **2017**, *403*, 472–486. [[CrossRef](#)]
22. Raimondi, A.; Girotti, G.; Blengini, G.A.; Fino, D. LCA of petroleum-based lubricants: State of art and inclusion of additives. *Int. J. Life Cycle Assess.* **2012**, *17*, 987–996. [[CrossRef](#)]
23. Bouchet, M.D.B.; Martin, J.; Le Mogne, T.; Bilas, P.; Vacher, B.; Yamada, Y. Mechanisms of MoS₂ formation by MoDTC in presence of ZnDTP: Effect of oxidative degradation. *Wear* **2005**, *258*, 1643–1650. [[CrossRef](#)]
24. Hutchings, I. Tribology: Friction and wear of engineering materials. *Mater. Des.* **1992**, *13*, 187. [[CrossRef](#)]
25. Dias, H.W.J. Extração Química da Grafita Turbostrática Gerada in situ Pela Dissociação do Carbetto de Silício em Matriz de Ferro puro Durante Tratamento Térmico de Sinterização. Ph.D. Thesis, Universidade Federal de Santa Catarina, Florianópolis, Brazil, 2019; 127p. (In Portuguese)
26. Damin, K.V.S.; Tasiar, G.D.R.; Lucena, A.C.; Bendo, T.; Hammes, G.; Klein, A.N.; De Mello, J.D.B.; Binder, C. Improvement of tribological properties of sintered self-lubricating composites produced by surface Mo-enrichment. *Wear* **2020**, *442–443*, 203123. [[CrossRef](#)]
27. Chieu, T.C.; Dresselhaus, M.S.; Endo, M. Raman studies of benzene-derived graphite fibers. *Phys. Rev. B* **1982**, *26*, 5867–5877. [[CrossRef](#)]
28. Ferrari, A.C.; Robertson, J. Interpretation of Raman spectra of disordered and amorphous carbon. *Phys. Rev. B* **2000**, *61*, 14095–14107. [[CrossRef](#)]
29. Ferrari, A.C. Raman spectroscopy of graphene and graphite: Disorder, electron–phonon coupling, doping and nonadiabatic effects. *Solid State Commun.* **2007**, *143*, 47–57. [[CrossRef](#)]
30. Cantarero, A. Raman Scattering Applied to Materials Science. *Procedia Mater. Sci.* **2015**, *9*, 113–122. [[CrossRef](#)]
31. Matassa, R.; Orlanducci, S.; Tamburri, E.; Guglielmotti, V.; Sordi, D.; Terranova, M.L.; Passeri, D.; Rossi, M. Characterization of carbon structures produced by graphene self-assembly. *J. Appl. Crystallogr.* **2014**, *47*, 222–227. [[CrossRef](#)]
32. Karthik, C.; Kane, J.; Butt, D.P.; Windes, W.E.; Ubic, R. Microstructural Characterization of Next Generation Nuclear Graphites. *Microsc. Microanal.* **2012**, *18*, 272–278. [[CrossRef](#)] [[PubMed](#)]
33. Ning, X.J.; Pirouz, P.; Lagerlof, K.P.D.; DiCarlo, J. The Structure of Chemically Vapour Deposited SiC Monofilaments. *Mater. Res.* **1990**, *5*, 2865–2876. [[CrossRef](#)]
34. Le Roux, H. An electron diffraction analysis of turbostratic graphite in cemented carbides. *Acta Metal* **1985**, *33*, 309–315. [[CrossRef](#)]
35. Kovalevski, V.; Buseck, P.R.; Cowley, J. Comparison of carbon in shungite rocks to other natural carbons: An X-ray and TEM study. *Carbon* **2001**, *39*, 243–256. [[CrossRef](#)]
36. Blau, P.J. How common is the steady-state? The implications of wear transitions for materials selection and design. *Wear* **2015**, *332–333*, 1120–1128. [[CrossRef](#)]
37. Bordignon, R.; Salvaro, D.; Binder, C.; Klein, A.N.; Drago, V.; De Mello, J.D.B. Tribological Behaviour of Plasma-Functionalized Graphene as Low-Viscosity Oil Additive. *Tribol. Lett.* **2018**, *66*, 114. [[CrossRef](#)]